Crystal Chemistry and Electronic Structure of the β-AlFeSi Phase from First-Principles

C. M. Fang*, Z. P. Que and Z. Fan

BCAST, Brunel University London, Kingston Lane, Uxbridge, Middlesex, UB8 3PH, UK

*Corresponding author: Changming Fang

E-amil: Changming.Fang@Brunel.AC.UK

Highlights

- Si prefers to substitute on the Al1 or Al6 site, forming β-$Al_{4.5}(Si,Al)^{I}Fe$ or β-$Al_{4.5}(Si,Al)^{VI}Fe$;
- Stacking of the FeAlSi blocks leads to phase transformations;
- Extra freedom permits more Si solute in the β-phase at the casting temperature;
- Electronically β-$Al_{4.5}SiFe$ is anisotropic with a narrow pseudo bandgap.

Graphical Abstract

Si solute on the Al1 or Al6 site, forming β-$Al_{4.5}Si^{I}Fe$ or β-$Al_{4.5}Si^{VI}Fe$ at low temperature. At casting temperature, the extra freedom allows more Si solute in the crystal. Stacking of the FeAlSi blocks of the layered β-$Al_{4.5}SiFe$ phase may lead to structural transformations.

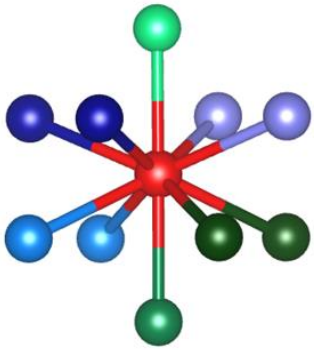

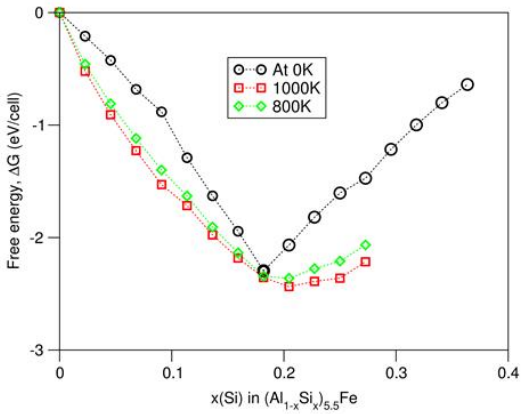

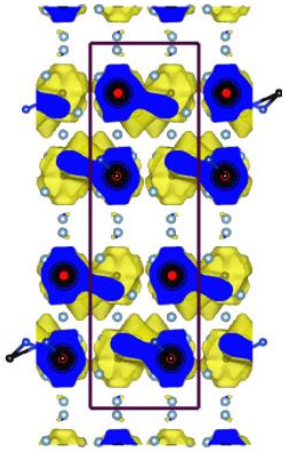

Abstract

β-AlFeSi has a layered structure composed of FeAlSi blocks and exhibits a rich variety of crystal chemistry. Plate-like/rod-like β-AlFeSi particles formed in Al-based alloys have nontrivial influences on the mechanical performance of the cast parts. Here, we investigate the stability, crystal chemistry and electronic structure of the β-phase using the first-principles density-functional theory (DFT) method. We reveal that Si prefers on the Al1 or Al6 sites, forming stable β-$Al_{4.5}Si^{I}Fe$ or β-$Al_{4.5}Si^{VI}Fe$ (the Roman numerals represent the Al sites in the Rømming's labels). This differs from the existing model with a homogeneous Si/Al distribution. Moreover, the calculations also find that stacking of the FeAlSi blocks leads to structural transformations. Electronically β-$Al_{4.5}$SiFe is anisotropic with a narrow pseudo-band-gap, indicating its unusual physical properties. The obtained information here sheds some light not only on the stability and crystal chemistry of the β-phase as a member of the large family of the Fe-containing intermetallic compounds in Al-based alloys, but also on its potential applications as low-dimensional functional materials.

Key words: Fe-intermetallic Compounds; Silicon Substitution; β-$Al_{4.5}$SiFe; *Ab-Initio* Calculations; Crystal Chemistry.

1. Introduction

As a family member of the Fe-containing intermetallic compounds (Fe-IMCs), β-AlFeSi has been a topic of intensive study due to both academic curiosity and industrial interest [1-15]. The β-phase has a list of names, $Al_9Fe_2Si_2$, Al_5FeSi, $Al_{4.5}FeSi$, β-AlFeSi, *etc*. in the literature [1-19]. Structurally β-AlFeSi is layered and exhibits a rich variety of crystal chemistry [11-15]. Its symmetry and crystal structure have been under discussions [10-15]. Currently it is accepted that the β-phase has a monoclinic lattice with space group A2/a (Nr. 15) [2, 12, 22, 15]. It contains seven crystallographically different atomic species (one Fe and six Al/Si) (Fig. 1). In this structural model the distribution of the Si atoms was treated to be homogeneous at the Al sites [11-15]. This indicates that the local symmetry in the crystal is broken in the atomic picture [23]. This Si/Al homogeneous distribution model has been applied in the structural determinations of the Fe-IMCs [2-6, 10-22]. Thus, knowledge about the accurate Si distribution in β-AlFeSi is helpful to get insight into the accurate structures of the Fe-IMCs, too. The structure of β-$Al_{4.5}FeSi$ is composed of building blocks (Fig. 1a). Each block is composed of centered Fe atoms coordinated by 10 Al/Si atoms (FeAlSi blocks) [11-15] (Fig. 1b). Different stackings of the blocks may change the lattice symmetry and form new phases [11-15, 24, 25]. Understanding of the accurate structure of β-AlFeSi sheds light on its phase relations with and phase transformations from/to the other Fe-IMCs during casting of Al-based alloys [6, 16]. Electronically the unique layered structure of β-AlFeSi indicates unusual physical properties with potential applications as low-dimensional functional materials. To reach this goal, knowledge about its accurate crystal structure including the Si distribution is the prerequisite. Metallurgically, both iron and silicon exist unavoidably in commercial Al metals and Al-based alloys as impurities. Iron has a low solid solubility (less than 0.05 percent) at equilibrium in Al [1, 2]. Thus, iron exist in aluminum-based alloys in the form of Fe-IMCs [1-4]. The formed Fe-IMCs particles, including β-AlFeSi exhibit various morphologies and may deteriorate the mechanical properties of cast parts. Information about the stability and structural properties of the harmful β-AlFeSi phase is useful to control/minimize its existence in cast products for various Al ingots including Al-scrap which contains various contents of iron and silicon. The latter is important for our environments and the recycling economy [3, 4, 6].

Experimental efforts for β-AlFeSi have been made mainly on preparation, phase characterization and structural analysis [2, 5-22, 24]. It is difficult for most diffraction methods to distinguish Si and Al in the Fe-IMCs, as they are neighbors in Periodic Table of Elements and differ from each other with only one-electron. Till now there has been no experimental report on the electronic properties of this layered compound, too. In these aspects, theoretical approaches, especially parameters-free first-principles methods are helpful. First-principles approaches have been successfully applied to investigate the stability and structural and electronic properties of many Fe-containing intermetallic compounds and precipitates [26-29], including Si preference on the atomic sites in θ-$Al_{13}Fe_4$ [26, 30]. Here we investigate Si distribution in and electronic structure of β-AlFeSi using a first-principles density-functional theory (DFT) approach. We reveal that the stable structure has a chemical composition of β-$Al_{4.5}SiFe$ with Si at specific Al sites. The crystal symmetry is strictly kept in the structural model. At the casting temperature, configuration entro-

py contribution enables more Si solute in β-$Al_{4.5}SiFe$. Electronically β-$Al_{4.5}SiFe$ is unusually anisotropic with a narrow pseudo-band-gap.

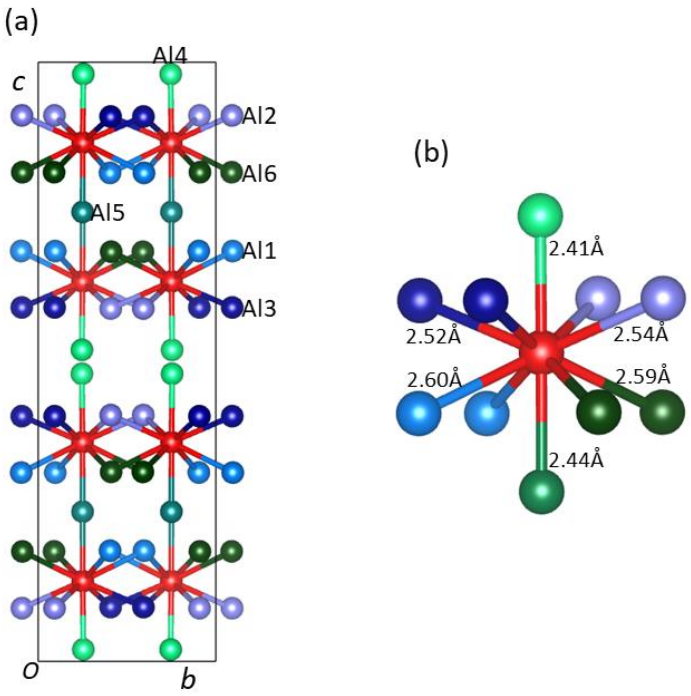

Fig. 1 (Color online) Schematic structure of β-($Al_{4.5}Si$)Fe along the [1 0 0] projection (a) [12] and the coordination of Fe by Al/Si atoms (b). The bond lengths in (b) are from the optimized structure for novel β-$Al_{5.5}Fe$ (see text). The red spheres represent Fe, the rest colored spheres represent the six Al (represents here for Al/Si) species [12] as labelled in (a).

2. Details of Calculation Methods

We performed first-principles calculations for the (novel) binary β-$Al_{5.5}Fe$ based on the structural model [12]. The formation energy here is defined as,

$$\Delta E(Al_{5.5}Fe) = E(Al_{5.5}Fe) - [5.5\,E(Al) + E(Fe)] \quad (1)$$

Here $E(Al_{5.5}Fe)$, $E(Al)$ and $E(Fe)$ are the total valence electron energies of β-$Al_{5.5}Fe$, the solid element α-Al and α-Fe, respectively. The unit of ΔE is eV/Fe or eV/f.u., where f.u. represents formular unit.

To have a measure of the relative stability of β-AlFeSi with respect to the parent intermetallic compound, β-$Al_{5.5}Fe$ and the elemental solids (α-Al and Si), the formation energy per cell for Si doping in the compounds is given by:

$$\Delta E_{Si}[(Al_{1-x}Si_x)_{5.5}(Fe] = E\{(Al_{1-x}Si_x)_{5.5}Fe\} - \{E(Al_{5.5}Fe) + 5.5\,x[E(Si) - E(Al)]\} \quad (2)$$

Here, $E\{(Al_{1-x}Si_x)_{5.5}Fe\}$ is the calculated energy of $(Al_{1-x}Si_x)_{5.5}Fe$ in the unit cell. The unit of the formation energy here is eV/cell.

At the temperature T = 0 K and the pressure p = 0 Pa, the enthalpy difference is equal to the energy difference, $\Delta H = \Delta E$, when the zero-point vibration contribution is not taken into account.

A negative value of the formation energy means that the formation is exothermal and this reaction is favored.

We utilized the first-principles code VASP (Vienna *Ab initio* Simulation Package) [31, 32]. This code employs the Density-Functional Theory (DFT) within the Projector-Augmented Wave (PAW) approach [33, 34]. The Generalized Gradient Approximation (GGA-PBE) [35, 36] was used for the exchange and correlation energy terms. The GGA works better for the transition metals including iron and related compounds than the Local Density Approximation (LDA) [29, 34-36]. We used a cut-off energy of 550 eV for the wave functions and the cut-off energy of 700 eV for the augmentation functions, which are notably higher than the corresponding default values (E_{MAX}/E_{AUG} = 240.3eV/291.1eV for Al, 267.9eV/511.4eV for Fe and 245.3eV/322.1eV for Si, respectively). The electronic wave functions were sampled with a dense, e.g. a 8×8×2 grid and 50 to 68 ***k***-points in the irreducible Brillouin zone (BZ) of β-AlFeSi and the related compositions depending on the symmetry, using the Monkhorst–Pack method [37]. First-principles structural optimizations were performed for both lattice parameters and atomic coordinates. Different ***k***-meshes and cut-off energies were first tested. The tests showed good convergence (<1meV per atom).

3. Results

Structure optimizations and total energy calculations were performed for the elemental solids using above settings. The calculations produced the lattice parameter, a = 4.039Å (experimental value 4.04325Å at 0K [38]) for α-Al, a = 2.831Å (experimental value 2.86072Å at 0K [38]) for α-Fe and a = 5.468Å (experimental value 5.43298Å at 0K [38]) for the cubic Si. The calculations reproduced well the experimental values at 0K.

3.1. Energies and structural properties of Si solute in the β-phase

We first performed structural optimizations for the novel binary β-$Al_{5.5}Fe$. The calculated formation energy is -1.267eV/Fe for β-$Al_{5.5}Fe$ according to Eq. 1. This energy is notably higher than that for θ-$Al_{13}Fe_4$ (-1.403eV/Fe) [26], indicating that β-$Al_{5.5}Fe$ is less stable than θ-$Al_{13}Fe_4$.

Next, we investigated the energies of intrinsic defects and Si solute, Fe or Al vacancies, replacements of Al by Fe, Fe by Al and Fe by Si in β-$Al_{5.5}Fe$. The definitions of the formation energies are from our previous work [26]. The calculations revealed high costs for formation of the intrinsic defects with respect to β-$Al_{5.5}Fe$ and the elemental solids: +1.244eV for an Fe vacancy, +1.240 to +1.1724eV to create a vacancy at an Al site. To replace one Fe by Al costs +1.170eV and replacing one Al by Fe costs +1.546 to +2.084eV. Moreover, replacement of one Fe by Si costs +1.407eV. Such high energy costs indicate highly unlikely of formation of these defects. This agrees with the previous work for the defects in θ-$Al_{13}Fe_4$ [26, 39, 40].

The calculations were performed for one Si substitution on the six Al sites. The obtained formation energies according to Eq. 2 are shown in Fig. 2 and in the supplementary materials, Table S-I.

The calculations showed that the formation energy of one Si substitution on Al1 is equal to that

on Al6 (Al1/Al6) and that at Al2 to that at Al3. The formation energies at the six Al sites can be classified into four groups: Al/Al6, Al2/Al3, Al4, Al5. The Si preference has the series (from high to low): Al1/Al6 > Al5 > Al2/Al3 > Al4. Each Al4 atom has one Fe neighbors whereas at the rest sites each Al has two Fe neighbors. This indicates that Si prefers the Al sites of more Fe neighbors. The lengths of the axis of cell volume decrease with Si solute at the Al sites, whereas the angle increases slightly (Table S-I).

The distinct preference of Si substitution at the Al sites except Al4 suggested additions of more Si atoms. The obtained dependences of the formation energies on Si content are shown in Fig. 2. We also performed structural optimizations and total energy calculations for full Si occupations on the Al sites. The results (formation energy, lattice parameters and important interatomic distances) are listed in Table I for the highly-stable ones and Table S-II for all the configurations.

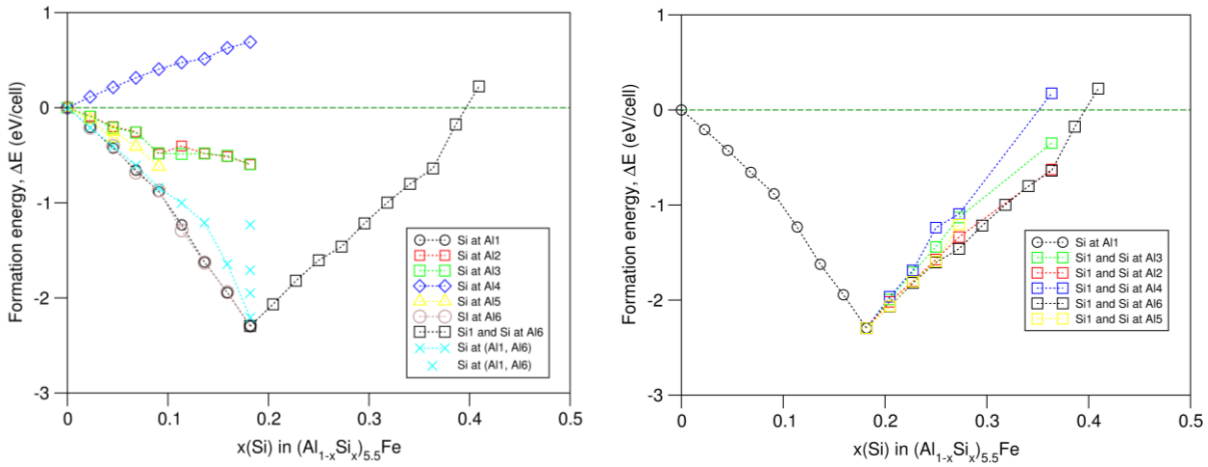

Fig. 2 (Color online) Formation energies of the β-phase with Si solutes at the Al sites from first-principles DFT-GGA calculations.

From the calculations we obtained the following conclusions:

1) The formation energies decrease with Si content on Al1/Al6, Al5, Al2/Al3 until each Al site is fully occupied by Si, whereas Si solute at the Al4 site is unfavored (Fig. 2a).

2) The configurations of the same Si content have the following order series (from high to low): Si(Al1/Al6) > Si(Al5)>Si(Al2/Al3) >> Si(Al4) (Fig. 2a).

3) At lower Si content (x < 4/44 in $(Al_{1-x}Si_x)_{5.5}Fe$), Si atoms occupy the Al1/Al6 sites randomly. At higher Si content, ordered Al1/Al6 configurations become more favored, especially for the configurations with x = 8/44.

4) The formation energy reaches its minimum for Si full occupation at the (Al1 or Al6), Al5 and (Al2 or Al3) sites, whereas it reaches a maximum for Si full occupation at the Al4 site (Fig. 2) and Table S-II. The most stable configurations are β-$Al_{4.5}Si^{I}Fe$ with Si at the Al1 sites and

β-$Al_{4.5}Si^{VI}Fe$ with Si at the Al6 sites. They are referred as β-$Al_{4.5}$SiFe. The calculated lattice parameters are in good agreement with the experimental values (<1%) (Table 1)

The calculations revealed that addition of extra Si into β-$Al_{4.5}$SiFe increases the formation energy at 0K (Fig. 2b). Low Si addition into the Al sites in β-$Al_{4.5}$SiFe has similar formation energies, whereas addition of more Si cause diversity of the formation (Fig. 2b). Interestingly, configurations with a full occupation of (Al1 and Al3), and (Al6 and Al2) are more stable than those of (Al1 and Al2), (Al6 and Al3). This is due to their local symmetry [12, 15].

Table I. The calculated results (lattice parameters and formation energies) for the novel binary β-$Al_{5.5}Fe$ and β-$Al_{4.5}$SiFe configurations of high stability with comparison with the experimental data in the literature. XRD represent the X-Ray Diffraction (technique); SAED Selected Area Electron Diffraction, EBED Convergent Beam Electron Diffraction. *This formation energy is per primitive unit cell.

Phase	lattice parameters(Å) *a*(Å), *b*(Å), *c*(Å), β(°), V_{cell}(Å^3)	Δ*E*(eV/cell) or expl. technique
β-$Al_{5.5}Fe$	6.240, 6.240, 21.087, 90.34, 821.13	-
β-$Al_{4.5}Si^{I}Fe$	6.164, 6.165, 20.768, 91.39, 788.91	-2.295
β-$Al_{4.5}Si^{VI}Fe$	6.165, 6.165, 20.766, 91.43, 788.98	-2.297
Experiment [12]	6.161, 6.175, 20.813, 90.42, 791.79	XRD, SAED
[13]	6.1676,6.1661,20.8093, 91, 791.26	SAED, CBED
β-$Al_{4.5}$SiFe (C_ii)	6.162, 6.169, 20.779, 90, 789.83	-2.220
Experiment [14]	6.18, 6.20, 20.8, 90, 796.97	SAED, CBED
[11]	6.184, 6.250, 20.69, 90, 799.67	CBED
β-$Al_{4.5}$SiFe (C_iii_1)	6.163, 6.166, 41.570, 90.15, 1579.63	-2.229
Experiment [41, 42]	6.12, 6.12, 41.5, 91, 1554.12	XRD
β-$Al_{4.5}$SiFe (C_iii_2)	6.164, 6.164,41.579 ,90, 1579.99	-2.228
Experiment [42]	6.18 , 6.18, 42.5, 90, 1617.92	XRD

Fig. 1 shows that along its *c*-axis, the β-$Al_{4.5}$SiFe unit cell consists of four FeAlSi blocks. Each block contains two Fe, two Si atoms and nine Al atoms, named as *q*-FeAlSi. The calculations showed the configurations with the Si atoms occupying both Al1 and Al6 sites in one *q*-FeAlSi block have formation energies over 1eV higher than that of the stable β-$Al_{4.5}$SiFe. It is also possible that one block has both Si atom either at Al1 (*q*-$FeAlSi^{I}$) or at Al6 (*q*-$FeAlSi^{VI}$). Then we investigate the formation energy and structure of different stackings by such blocks: Configurations i) (C_i) has a stacking of -(*q*-$FeAlSi^{I}$)-(*q*-$FeAlSi^{VI}$)-(*q*-$FeAlSi^{I}$)-(*q*-$FeAlSi^{VI}$)- series; C_ii) has a stacking series -2(*q*-$FeAlSi^{I}$)-2(*q*-$FeAlSi^{VI}$)- in the unit cell; and C_iii) has a -4(*q*-$FeAlSi^{I}$)-4(*q*-$FeAlSi^{VI}$)- in a $1a_0 \times 1b_0 \times 2c_0$ supercell, where a_0, b_0, c_0 are the lattice parameters of the convention cell of the β-phase.

The calculations showed that for C_i) the lattice becomes orthorhombic with *a* = 6.1522Å, *b* = 6.1554Å, *c* = 20.9332Å. However, the formation energy is 1.034eV higher than the most stable ones, indicating this configuration is unlikely.

For C_ii) the optimized lattice becomes orthorhombic with parameters, *a* = 6.1616Å, *a* = 6.1692Å, *c* = 20.7786Å. Moreover, the formation energy (-2.220eV/cell) is slightly higher than

that of the most stable configuration (energy difference of 0.076eV/cell, Fig. 2a)), indicating that this type of stackings is highly likely. The obtained lattice parameters are close to those experimental observations [11, 14].

As shown in Table for the supercell, the structural optimizations produced two replacements of almost identical energy: C_iii_1) is a monoclinic lattice with lattice parameters: a = 6.163Å, b = 6.166Å c = 41.570Å and β = 90.15°; C_ii_2): a tetragonal lattice (fixed) with a = 6.164Å, c = 41.579Å. There are slight anisotropic pressures along its a-, b- and c-axis with values -0.47kB, +0.25kB, -0.53kB, respectively. As shown in Table I, the early experiments produced scattering values. The small length-differences of the in-plane-axis and the small angle deviation from 90° might be not accurately determined in the early experiments [41, 42].

The calculations showed that the building unit is the double-(q-FeAlSi) slab which is connected to the neighboring slabs via Al5 atoms (Fig. 1). The changes of lattice symmetry for the configurations with stackings of the double-(q-FeAlSi) blocks help to understand the reported structural models [11-15, 41, 42].

Next we address the dependences of lattice parameters of the highly stable configurations of the β-phase on Si content. The dependences of the lattice parameters and cell volume for the stable configurations are plotted in Fig. S-1.

The lengths of the in-plane axis, a and b decreases with increasing Si concentrations. The cell volume decreases almost linearly with Si concentration. Meanwhile, the length of c-axis and the angle have unusual dependences. The length of c-axis decreases with Si concentration and reaches it minimum at x = 18.18% and then increases with further addition of Si, whereas the angle behaves oppositely: with Si content, it increases first and reaches a maximum at x = 18.18% and then decreases.

In brief, the first-principles calculations revealed Si preference at the Al1 or Al6 sites, forming stable β-$Al_{4.5}Si^{I}Fe$ or β-$Al_{4.5}Si^{VI}Fe$. The calculated lattice parameters agree with the experimental values. The stackings of the double-(q-FeAlSi) blocks result in highly-stable configurations of orthorhombic or tetragonal lattices.

3.2. Chemical bonding in β-$Al_{4.5}$SiFe

Here we analyze the structure of and chemical bonding in β-$Al_{4.5}$SiFe in detail. The lattice parameters were listed in Table 1. The atomic coordinates and important interatomic distances for β-$Al_{5.5}$Fe and β-$Al_{4.5}Fe^{I}Si$ and β-$Al_{4.5}Fe^{VI}Si$ are listed in Table II and Table III, respectively.

Table II. Calculated atomic coordinates and charges at the atomic sites for β-$Al_{5.5}$Fe and ternary β-$Al_{4.5}Fe^{I}Si$ and β-$Al_{4.5}Fe^{VI}Si$ with comparison with the available experimental data [12]. The corresponding lattice parameters are listed in Table I. # represent site occupied by Si and * the Si/Al are homogeneously distributed at the Al sites [12].

	β-$Al_{5.5}$Fe	β-$Al_{4.5}Si^{I}Fe$	β-$Al_{4.5}Si^{VI}Fe$	Exptl. [12] β-($Al_{4.5}$Si)Fe
Species	Coordinates /charge (e/atom)	Coordinates /charge (e/atom)	Coordinates /charge (e/atom)	Coordinates
Fe, 8f	0.5021, 0.2507, 0.1341 /-3.65	0.4937, 0.2559, 0.1367 /-3.17	0.5063, 0.2441, 0.1367 /-3.16	0.5024, 0.2605, 0.1367
Al1, 8f	0.3458, 0.5957, 0.1848 /0.63	0.3389, 0.5943, 0.1811# /-1.43	0.3642, 0.6134, 0.1899 /1.27	0.3583, 0.6062, 0.1863*
Al2, 8f	0.3432, 0.9083, 0.0889 /0.85	0.3306, 0.9187, 0.0930 /1.11	0.3419, 0.9093, 0.0890 /1.18	0.3387, 0.9116, 0.0897*
Al3, 8f	0.1593, 0.4075, 0.0907 /0.87	0.1576, 0.4087, 0.0891 /1.19	0.1692, 0.4183, 0.0933 /1.12	0.1669, 0.4167, 0.0908*

Al4 8f,	0.4992, 0.2539, 0.0200 /0.24	0.5093, 0.2455, 0.0187 /0.30	0.4906, 0.2562, 0.0186 /0.29	0.4972, 0.2666, 0.0181*
Al5,4d	0.5000, 0.2500, 0.2500 /0.85	0.5000, 0.2500, 0.2500 /1.44	0.5000, 0.2500, 0.2500 /1.44	0.5000, 0.2500, 0.2500*
Al6, 8f	0.1603, 0.0893, 0.1837 /0.66	0.1359, 0.1127, 0.1898 /1.27	0.1612, 0.0939, 0.1810[#] /-1.44	0.1526, 0.1000, 0.1836*

As shown in Table II, the calculated lattice parameters for the β-$Al_{4.5}Si^{I}Fe$ are identical to those of β-$Al_{4.5}Si^{VI}Fe$ in the numerical error, except for the exchange of Si1/Si6 sites. There is an excellent agreement (within 0.5%) between the calculations and experimental values. For the same species the atomic coordinates in the different configurations/phases in Tale II are generally close each other. The atomic coordinates for Al6 in β-$Al_{4.5}Si^{I}Fe$ and Al1 in β-$Al_{4.5}Si^{VI}Fe$ display more pronounced differences than those in other configurations. This is due to the Si solutes.

Table III. The interatomic distances within 3.0Å in β-$Al_{5.5}Fe$ and β-$Al_{4.5}Fe^{I}Si$ and β-$Al_{4.5}Fe^{VI}Si$ with comparison with the available experimental data [12]. *In [12] the Si atoms are homogeneously distributed at the Al sites.

	β-$Al_{5.5}Fe$	β-$Al_{4.5}Fe^{I}Si$	β-$Al_{4.5}Fe^{VI}Si$	Exp.[12]*
Fe	-10Al: 2.14, 2.44, 2.52(×2), 2.54(×2), 2.56, 2.58, 2.59, 2.60	-8Al: 2.35, 2.45, 2.49(×3), 2.50, 2.60, 2.68 -2Si: 2.46, 2.52	-8Al:2.35, 2.45, 2.49(×2), 2.50(×2), 2.60, 2.69 -2Si:2.46, 2.52	-10Al:2.358, 2.434, 2.467, 2.468, 2.531, 2.534,2.553, 2.572, 2.596,2.598
Al1 (Si1)	-2Fe: 2.58, 2.60 -7Al: 2.58, 2.73, 2.74, 2.77, 2.78, 2.80, 2.81	(Si1)-2Fe: 2.46, 2.52 -7Al: 2.51, 2.58, 2.68, 2.69, 2.71(×2), 2.76	-2Fe: 2.60, 2.69 -5Al: 2.61, 2.69, 2.73, 2.78, 2.79 -2Si: 2.58, 2.69	-2Fe: 2.534, 2.553 -7Al: 2.566, 2.583, 2.708, 2.709, 2.731, 2.758, 2.764
Al2	-2Fe: 2.54(×2) -7Al: 2.57, 2.70, 2.78(×2), 2.79, 2.80, 2.81	-2Fe: 2.49(×2) -6Al: 2.61, 2.70, 2.74, 2.75, 2.79, 2.85 -Si: 2.71	-2Fe: 2.50(×2) -5A: 2.68, 2.76, 2.77, 2.78, 2.85. -2Si: 2.51, 2.71	-2Fe: 2.531, 2.596 -7Al: 2.553, 2.702, 2.740, 2.758, 2.795, 2.829, 2.863
Al3	-2Fe: 2.52(×2) -7Al: 2.58, 2.70, 2.77(×2), 2.79(×2), 2.80	-2Fe: 2.49, 2.50 -5Al: 2.68, 2.75, 2.77, 2.78, 2.85 -2Si: 2.51, 2.71	-2Fe: 2.49(×2) -6Al: 2.61, 2.69, 2.74, 2.75, 2.79, 2.85 -1Si: 2.71	-2Fe: 2.434, 2.467 -6Al: 2.583, 2.642, 2.680, 2.708, 2.750, 2.764
Al4	-1Fe: 2.41 -7Al: 2.70(×2), 2.77(×2), 2.78(×2), 3.18	-Fe: 2.45 -6Al: 2.68, 2.70, 2.74, 2.75(×2), 2.77	-1Fe: 2.45 -6Al: 2.68, 2.69, 2.74, 2.75, 2.76, 2.77	-1Fe: 2.468 -7Al: 2.642, 2.680, 2.702, 2.708, 2.795, 2.829, 2.979
Al5	-2Fe: 2.44(×2) -8Al: 2.72(×2), 2.73(×4), 2.74(×2)	-2Fe: 2.35(×2) -4Al: 2.69(×2), 2.73(×2) -4Si: 2.68(×2), 2.76(×2)	-2Fe: 2.35(×2) -4Al: 2.69(×2), 2.73(×2) -4Si: 2.68(×2), 2.76(×2)	-Fe: 2.358(×2) -8Al: 2.702(×2), 2.709(×2), 2.731(×2), 2.735(×2)
Al6 (Si6)	-2Fe: 2.56, 2.59 -7Al: 2.57, 2.72, 2.73, 2.77, 2.78, 2.79, 2.80	-2Fe: 2.60, 2.68 -5Al: 2.61, 2.69, 2.73, 2.78, 2.79 -2Si: 2.58, 2.69	(Si6)-2Fe: 2.46, 2.52 -7Al: 2.51, 2.58, 2.68, 2.69, 2.71(×2), 2.76	-2Fe: 2.572, 2.598 -7Al: 2.553, 2.566, 2.702, 2.708, 2.735, 2.740, 2.750,

Table III shows that the Fe atoms in the β-phase have eight Al and two Si neighbors, or 10 Al/Si as in Fig. 1b. This coordination number (CN) is between that of α-Fe (CN = 8) and α-Al (CN = 12). The interatomic Fe-Al distances in the binary are in the range between 2.14Å and 2.60Å, which is smaller than that in the ternary configurations 2.35Å and 2.69Å. The latter is closer to the experimentally observed values from 2.36Å and 2.60Å. The Fe-Si distances are about 2.5 Å, between those of the Fe-Al bonds. It is also noted that in the binary β-$Al_{5.5}Fe$, the two Fe-Al bonds have the same length for Al2, Al3 and Al5, whereas they have different lengths for Al1 and Al6. This may relate to the lower formation energy for β-$Al_{4.5}Si^{I}Fe$ and for β-$Al_{4.5}Si^{VI}Fe$ as compared with for β-$Al_{4.5}Si^{II}Fe$, β-$Al_{4.5}Si^{III}Fe$ and for β-$Al_{4.5}Si^{V}Fe$.

3.3. Electronic properties of the β-$Al_{4.5}Si^{I}Fe$

Electronic structure calculations were performed for both β-$Al_{4.5}Si^{I}Fe$ and β-$Al_{4.5}Si^{VI}Fe$. The obtained electron density distribution in β-$Al_{4.5}Si^{I}Fe$, and related partial density of states of the atoms (pDOS) and total density of states (tDOS) for β-$Al_{4.5}Si^{I}Fe$ are shown in Fig. 3a and Fig. 3b, respectively. Fig. 4 shows the dispersion curves near the Fermi level (at 0eV) along the high symmetry lines in the Brillouin zone (BZ) of β-$Al_{4.5}Si^{I}Fe$.

Fig. 3a shows clear layered characteristics of β-$Al_{4.5}Si^{I}Fe$. In plane the Fe-Si form clusters which connected with each other, indicating covalent nature between them. Fig. 3a also showed that along the *z*-axis, the FeAlSi blocks in the first half of the cell are closer with each other, forming a slab which is well-separated from the other slab in the other half of the cell. This corresponds to the calculations for the highly-stable configurations with the stackings of the double(*q*-FeAlSi) blocks in Table I.

The Si/Al 3s, 3p states are all-over the valence and conduction bands. The Si 3s states are mainly at -11.6eV to -7.6eV. The upper part of the valence band is dominated by Al/Si 3p and Fe 3d states. Fig. 3b shows that the Fe 3d states dominates the upper part valence band with high densities range from -2.0eV to -0.5eV (Fig. 3b). This agrees with states with small dispersion in this energy range as shown in Fig. 4.

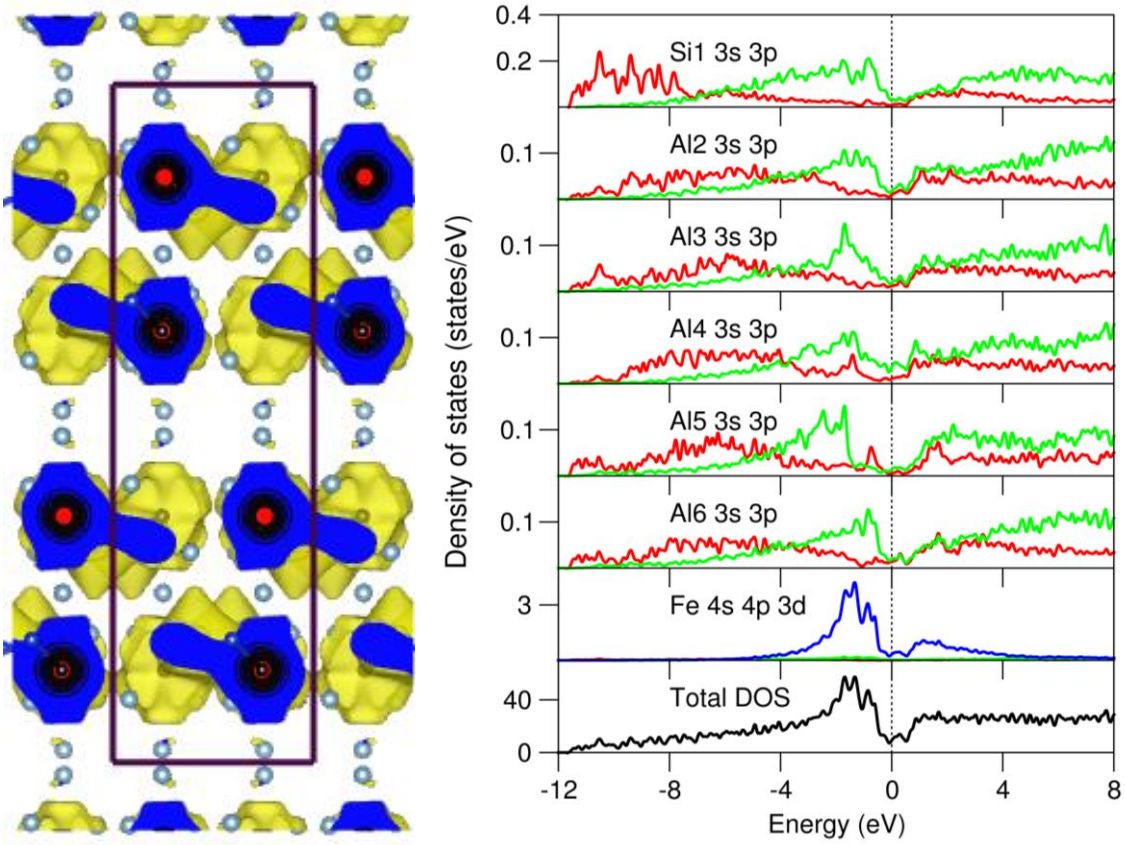

(a) (b)

Fig. 3 (Color online) The electron density distribution with iso-surface density (ρ0(r) = 0.04e/Å^3) (a) and partial and total density of states (b) of β-$Al_{4.5}Si^{I}Fe$. The latter was compared with those of β-$Al_{4.5}Si^{VI}Fe$

in Fig. S-2. In (a) the red/black-regions represent the atomic cores of Fe, the yellow clouds represent the iso-surfaces, the blue regions have higher valence-electrons; and the silvery spheres represent Al.

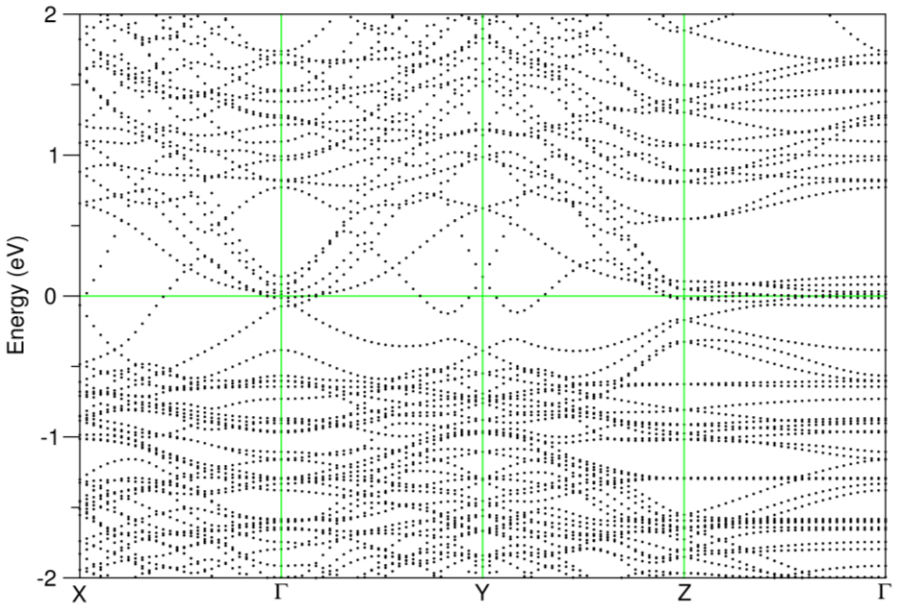

Fig. 4 (Color online) The dispersion curves along the high symmetry lines in the Brillouin zone of β-$Al_{4.5}Si^{I}Fe$, which can be regarded as pseudo-orthorhombic. The curves with a broad energy window is shown in Fig. S-3. The Fermi level is at 0eV.

As shown in Fig. 4, the dispersion curves along the in-plane directions (X-Γ-Y) show large dispersions with 1eV to 2eV, whereas the dispersion along the z-axis (Z- Γ) is small, typically about 0.1 to 0.2eV. Even taking into the ratio of axis lengths (c/a ~ 3.37) in account, this anisotropy is still to be about 3:1. Thus, β-$Al_{4.5}Si^{I}Fe$ is anisotropic of the electrical and thermal transport properties. Analysis showed that the states at the Fermi level at Γ in the Brillouin Zone are dominated by Al/Si p and Fe d characters.

There is a fall of total DOS at the Fermi level with low density of states at -0.5 to 0.5eV (Fig. 3b). The band structure (Fig. 4) also show few states in this energy range. The lower part of conduction band is dominated by Al/Si 3p and some Fe 3d states. We refer such a unusual low DOS at the Fermi level as a pseudo-gap [43]. Such narrow pseudo band-gap indicates unusual electronic properties and potential applications such as thermoelectric materials [43].

To get some direct impression about chemical bonding, we performed charge analysis using Bader's model [44, 45], in which the borders between one atom and its neighbors is defined by the 'zero-flux' surfaces of the gradient electron density. The obtained charges at the atomic sites for the most stable configurations are listed in Table II.

Charge transfer occurs from Al to Fe in β-$Al_{5.5}Fe$ (Table II). The amount of charging at the Al sites vary: about 0.65e/Al at Al1 and Al6, 0.86e at Al2 and Al3. The Al5 atoms loss the largest, 0.85e/Al whereas Al4 atoms loss just 0.24e/Al. The latter has less Fe neighbor (Table I).

The Si atoms derive electrons from Fe and Al: $Fe^{-3.65}$ in β-$Al_{5.5}Fe$ to $Fe^{-3.17}$ in β-$Al_{4.5}SiFe$. Correspondingly the Al atoms in β-$Al_{4.5}SiFe$ lose more electrons with comparing to those in β-

$Al_{5.5}Fe$, particularly the Al5. This indicates that the Al5 sites have higher attraction for Si, agreeing with the calculations in Fig. 2b. Such charge transfer at the atomic spheres is in lines with the electronegativity values of the elements (1.90 for Si, 1.83 for Fe and 1.60 for Al in the Pauling's scale).

4. Discussion

As shown in Figs. 1 and 3, β-$Al_{4.5}SiFe$ has a layered structure composed of *q*-FeAlSi blocks. Each Fe is coordinated by eight Al and two Si, being sandwiched by two layers of the Al(Si)1/Al(Si1)6 and Al2/Al3 atoms and topped/bottomed by an Al5 and Al4. The calculations showed that the Si prefers the Al1 or Al6 sites, forming β-$Al_{4.5}SiFe$. Such substitutions are partially due to the chemical pressure effects [46] as Si has a smaller atomic size than that of Al. The electronic band-structure calculations showed that the electronic structure exhibits low-dimensional character with a unusual narrow pseudo band-gap. This indicates that β-$Al_{4.5}SiFe$ has unusual physical properties and can be used as low-dimensional functional materials [43, 47].

The structural flexibility of β-$Al_{4.5}SiFe$ permits different stackings of the building a double-(*q*-FeAlSi) (half of the cell) slabs. Different stacking produces highly stable structures of an orthorhombic even tetragonal unit cell. This result helps us get into insight the variety of the lattices of this compound in the literature [12-15, 41, 42]. This deserves further investigation.

For most Al metals and Alloys casting occurs at typically 550°C to 700°C. At such temperature thermodynamics, including extra freedom or configurational entropy contribution plays a role in the formation and stability of the Fe-IMCs. The crucial role of configurational entropy contribution to the stability of alloys compounds at elevated temperature was discussed in the metals-alloyed mono-oxides, e.g. $(Mg_{1-x}A_x)O$ (A = Cd, Zn) [48, 49]. Our calculations showed that structural openness of the β-phase that there are two configurations for the most stable at 0K. According to thermodynamics, the free energy of a system at elevated temperature is: $\Delta G = \Delta H - T\,\Delta S_{conf.}$, here $\Delta H = \Delta E$ is the formation energy with ignorance of the zero-point energy, and $\Delta S_{conf.} = R \ln w$ (R is the Boltzmann's constant, w the number of configurations) is the configuration energy entropy here. To assess the number of freedom for one composition, we consider the configurations with energy different smaller than 0.3eV/cell based on the first-principles calculations. Details of the obtained results are listed in Table S-III. The dependences of free energies at 0K, 800K and 1000K are plotted in Fig. 5.

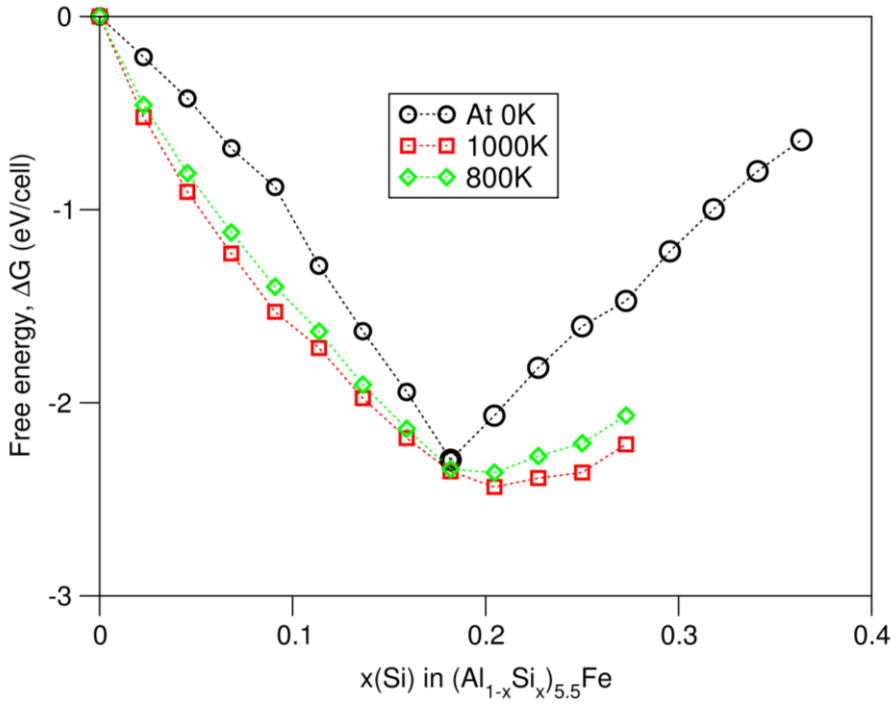

Fig. 5 (Color online) Dependences of free energies of the β-phase on Si contents at 0K, 800K and 1000K (Table S-III).

The Si content range in the β-phase depends pronouncedly on the temperature. Apparently at low temperature, the β-phase has composition formula $Al_{4.5}SiFe$. At 1000K, the Si content range from x = 0.182 to 0.250. Meanwhile at 800K the Si content range becomes smaller (x = 0.182 to 0.215) with the minimum of free energy at x = 0.205 as shown in Fig. 5.

The experiments showed that during the casting of Al-Fe-Si alloys, the θ-phase particles form first [16]. Then, the β-phase or α-phase forms, depending on the chemical composition and casting conditions. Experiments also showed influences of Si contents on the related reactions [16]. To get insight into these reactions, we investigate the formation energies of the Al-rich Fe-IMCs, Al_6Fe, θ-$Al_{13}Fe_4$ and the β-phase with/without Si solute. The calculated formation energies with respect to the elemental solids, α-Al, α-Fe and FCC Si are listed in Table IV. Table IV also includes the formation energies of dilute Si and Fe in α-Al.

Table IV. The comparison of the formation energies per Fe in the related phases with/without Si solute. The data are from this work except of those labelled with references.

Formula	Δ*E*(eV/Fe)	Formula	Δ*E*(eV/Fe)
Si solute in α-Al	+0.431eV/Si [26]	-	
Fe solute in α-Al	-0.457 [26, 36]	-	-
Al_6Fe	-1.373 [39]	$(Al_{0.983}Si_{0.0417})_6Fe$	-1.286
β-$Al_{5.5}Fe$	-1.267	β-$Al_{4.5}FeSi$	-1.554
θ-$Al_{13}Fe_4$	-1.403	θ-$(Al_{0.949}Si_{0.051})_{13}Fe_4$ [26]	-1.410

The calculations showed that Si solute in Al_6Fe decreases its stability (Table IV) and thus, is unlikely. Si substitution at the Al sites in both θ-$Al_{13}Fe_4$ and the β-phase enhances their stability. Table IV shows that the binary (novel) β-$Al_{5.5}Fe$ structure is notably less stable than Al_6Fe and θ-

$Al_{13}Fe_4$. The high Si substitution in β-phase (15.38at.%) strongly enhances the stability of this phase that it becomes significantly more stable than the θ-phase with about 3.9at.%.

The higher stability of the θ-phase with small amount of Si enables it form first in Al-Fe-Si alloys. Lower temperature drives more Si into Fe-IMCs due to the energy cost of Si in solid Al (Table IV). This stabilizes other Fe-IMCs, such as the β-phase as the observed reaction: L + θ-phase → β-phase [16].

The obtained information about the accurate crystal structure, formation energies of β-$Al_{4.5}$SiFe is helpful to get insight into the phase formation and phase transformation in the casting of Al-based alloys. This study also enhances our understanding of the thermodynamics and crystal structures of complex Fe-IMCs formed on solidification of Al-based alloys [1, 16, 19-21, 39].

5. Conclusions

In this study, we investigated the structure chemistry and electronic properties of the β-AlSiFe phase of layered structure. The study revealed that i) Si prefers substitution on the Al1 or Al6 sites, forming stable β-$Al_{4.5}Si^{I}Fe$ or β-$Al_{4.5}Si^{VI}Fe$, which updated the widely used model with a homogeneous Si/Al distribution; ii) Analysis showed that extra freedom permits higher Si contents in β-$Al_{4.5}$SiFe at the casting temperature, in line with the variation of Si contents in the crystallites in cast Al-alloys in the literature; iii) Stacking of the building blocks (slabs) produces highly stable structures of different symmetry; iv) The electronic band structure of β-$Al_{4.5}$SiFe is anisotropic and has a pseudo band gap, indicating unusual physical properties.

Acknowledgements

Financial support from EPSRC (UK) under grant numbers EP/N007638/1 and EP/S005102/1 is gratefully acknowledged.

References

1). L. F. Mondolfo, *Aluminum Alloys: Structure and properties*, Butterworths, London (1976).

2). W. Khalifa, F. H. Samuel and J. E. Gruzleski, Iron intermetallic phases in the Al corner of the Al-Si-Fe system. Metall. Mater. Trans. A 34 (2003) 807-825.

3). B. J. M. Freitas, L. B. Otani, C. S. Kiminami, W. J. Botta and C. Bolfarini, Effect of iron on the microstructure and mechanical properties of the spray-formed and rotary-swaged 319 aluminum alloy, Intern. J. Adv. Manufacturing Technol. 102 (2019) 3879-3894.

4). L. F. Zhang, J. W. Gao, L. Nana, W. Damoah and D. G. Robertson, Removal of iron aluminum: A review, Mineral Processing & Extractive Metall. Rev. 33 (2012) 99-157.

5). N. C. W. Kuijpers, E. J. Vermolen, C. Vuik, P. T. G. Koenis, K. E. Nilsen and S. van der Zwaag, The dependence of the β-AlFeSi to α-Al(FeMn)Si transformation kinetics in Al-Mg-Si alloys on the alloying elements, Mater. Sci. Engin. A 394 (2005) 9-19.

6). Z. P. Que and C. L. Mendis, Heterogeneous nucleation and phase transformation of Fe-rich intermetallic compounds in Al-Mg-Si alloys, J. Alloys and Compounds 836 (2020) 155515.

7). S. K. Tang and T. Sritharan, Morphology of β-AlFeSi intermetallic in Al-7Si alloy castings. Mater. Sci. Techn. 14 (1998) 738–742.

8). X. Cao and J. Campbell, Morphology of β-Al_5FeSi phase in Al-Si cast Alloys. Mater. Trans. 47 (2006) 1303–1312.

9).D. Ferdian, C. Josse, P. N'Guyen, N. Gey, N. Ratel-Ramond, P. de Parseval, Y. Thebault, B. Malard, J. Lacaze and L. Salvo, Chinese Script vs Plate-Like Precipitation of β-$Al_9Fe_2Si_2$ Phase in an Al-6.5Si-1Fe Alloy. Metall. Mater. Trans. A 46A (2015) pp.2814-2818.

10). M. V. Kral, A crystallographical identification of intermetallic phases in Al-Si alloys, Mater. Lett. 59 (2005) 2271-2276.

11). G. J. Carpenter, and Y. Lepage, Revised cell data for the β-FeSiAl phase in aluminum alloys, Scripta Metall. Mater. 28 (1993) 733–736.

12). C. Rømming, V. Hansen and J. Gjønnes, Crystal structure of β-$Al_{4.5}FeSi$, Acta Cryst. B50 (1994) 307-312.

13). V. Hansen, B. Hauback, M. Sundberg, C. Rømming, J. Gjønnes, β-$Al_{4.5}FeSi$: A combinaed synchrotron powder diffraction, electron diffraction, high-resolution electron microscopy and single-crystal x-ray diffraction study of a faulted structure, Acta Crystal. B54 (1998) 351-357.

14). J. G. Zheng, R. Vincent and J. W. Steeds, Crystal structure of an orthorhombic phase in β-(Al-Fe-Si) precipitates determined by convergent-beam electron diffraction, Philos. Mag. A 80 (2000) 493-500.

15). H. Becker, T. Bergh, P. E. Vullum, A. Leineweber and Y. Li, β- and δ-Al-Fe-Si intermetallic phase, their intergrowth and polytype formation, J. Alloys and Compounds, 780 (2019) 917-929.

16). Z. P. Que and C. L. Mendis, Formation of θ-$Al_{13}Fe_4$ and the multi-step phase transformations to α-Al_8Fe_2Si, β-Al_5FeSi and δ-Al_4FeSi_2 in Al-20Si-0.7Fe alloy, Intermetallics 127 (2020) 106960.

17). Y. H. Cho, H. C. Lee, K. H. Oh, and A. K. Dahle, Effect of strontium and phosphorus on eutectic Al-Si nucleation and formation of β-Al_5FeSi in hypoeutectic Al-Si foundry alloys, Metall. Mater. Trans. A 39 (2008) 2435-2448.

18). L. Lu and A. K. Dahle, Iron-rich intermetallic phases and their role in casting defect formation in hypoeutectic Al-Si alloys. Metall. Mater. Trans. A 36 (2005) 819-835.

19). V. Raghavan, Al-Fe-Si (Aluminum-Iron-Silicon), J. Phase Equilibria 23 (2002) 362-366.

20). G. Ghosh, *Aluminium – Iron – Silicon*, G. Effenberg, S. Ilyenko (ed.), SpringMaterials, Landolt-Börnstein – Group IV Physical Chemistry 11D1 (2008).

21). M. C. J. Marker, B. Skolyszewska-Kühberger, H. S. Effenberger, C. Schmetterer and K. W. Richter, Phase equilibria and structural investigations in the system Al-Fe-Si, Intermetallics 19 (2011) 1919-1929.

22). S. Murali, K. S. Raman, and K. S. S. Murthy, Morphological studies on ß-$FeSiAl_5$ phase in Al- 7Si-0.3Mg alloy with trace additions of Be, Mn, Cr, and Co. Mater. Charact. 33 (1994) 99–112.

23). C. M. Fang, G. A. de Wijs, E. orhan, G. de With, R. A. de Groot, H. T. Hintzen and R. Marchand, Local structure and electronic properties of $BaTaO_2N$ with perovskite-type structure J. Phys. Chem. Solids, 64 (2003) 281-286.

24). M. V. Kral, A crystallographic identification of intermetallic phases in Al-Si alloys. Mater. Lett. 59 (2005) 2271-2276.

25). M. V. Kral, H. R. Mcintyre and M. J. Smillie, Identification of intermetallic phases in a eutectic Al-Si casting alloy using electron backscatter diffraction pattern analysis. Scripta Mater. 51 (2004) 215-219.

26). C. M. Fang, Z. P. Que, A Dinsdale and Z. Fan, Si solution in θ-$Al_{13}Fe_4$ from first-principles, Intermetallics 126 (2020) 106939.

27). C. Wolverton and V. Ozoliņš, Entropically favored ordering: The metallurgy of Al_2Cu revisited, Phys. Rev. Lett. 86 (2001) 5518-5521.

28). J. Ledieu, Ė. Gaudry, L. N. Loli, S. A. Villaseca, M. C. de Weerd, M. Hahne, P. Gille, J. M. Dubois and V. Fournée, Structural investigation of the (010) surface of the $Al_{13}Fe_4$ catalyst, Phys. Rev. Lett. 110 (2013) 076102.

29). C. M. Fang, M. H. F. Sluiter, M. A. van Huis, C. K. Ande and H. W. Zandbergen, Origin of predominance of cementite among iron carbides in steel at elevated temperature, Phys. Rev. Lett. 105 (2010) 055503.

30). J. Grin, U. Burkhard, M. Ellner and K. Peters, Refinement of the Fe_4Al_{13} structure and its relationship to the quasihomogical homeotypical structures, Z. Kristal. 209 (1994) 479-487.

31). G. Kresse and J. Hafner, *Ab initio* molecular-dynamics simulation of the liquid-metal-amorphous-semiconductor transition in germanium, Phys. Rev. B49 (1994) 14251-14269.

32). G. Kresse and J. Furthmüller, Efficiency of *ab-initio* total energy calculations for metals and semiconductors using a plane-wave basis set, Comp. Mater. Sci. 6 (1996) 15-50.

33). P. E. Blöchl, Projector augmented-wave method, Phys. Rev. B50 (1994) 17953-17978.

34). G. Kresse and J. Joubert, From ultrasoft pseudopotentials to the projector augmented-wave method, Phys. Rev. B59 (1999) 1758-1775.

35). J. P. Perdew, K. Burke and M. Ernzerhof, Generalized gradient approximation made simple, Phys. Rev. Lett. 77 (1996) 3865-3868.

36). C. M. Fang, M. A. van Huis, M. H. F. Sluiter and H. W Zandbergen, Stability, structure and electronic properties of γ-Al23Fe6 from first-principles theory, Acta Mater. 58 (2010) 2968-2977.

37). H. J. Monkhorst and J. D. Pack, Special points for Brillouin-zone integrations, Phys. Rev. B13 (1976) 5188-5192.

38). J. Arblaster, *Selected values of the crystallographic properties of the elements*, ASM International, Materials Park, Ohio 2018.

39). C. M. Fang, A. Dinsdale, Z.P. Que and Z. Fan, Intrinsic defects in and electronic properties of θ-$Al_{13}Fe_4$: An *ab initio* DFT study, J. Phys. Materials 2 (2019) 015004.

40). A. Dinsdale, C. M. Fang, Z. P. Que and Z. Fan, Understanding the thermodynamics and crystal structure of complex Fe containing intermetallic phases formed on solidification of Aluminium alloys, JOM (2019) 1731-1736.

41). G. Phragmen, On the phases occurring in alloys of aluminium with copper, magnesium, manganese, iron, and silicon, J. Inst. Met. 77 (1950) 489-552.

42). P.J. Black, XLIX. Brillouin zones of some intermetallic compounds, The London, Edinburgh, and Dublin Philosophical Magazine and Journal of Science 46 (1955) 401-409.

43). Z. T. Tian, S. Lee and G. Chen, Comprehensive review of heat transfer in thermoelectric materials and devices, Annual Review of Heat transfer 17 (2014) 426-483.

44). R. F. W. Bader, A bonded path: A universal indicator of bonded interactions, J. Phys. Chem. A (1998) 7314-7323.

45). G. Henkelman, A. Arnaldsson and H. Jónsson, A fast and robust algorithm for Bader decomposition of charge density, Comp. Mater. Sci. 36 (2006) 354-360.46). K. P. Hilleke, R. T. Fredrickson, A. I. Vinokur and D. C. Fredrickson, Substitution patterns understood through chemical pressure analysis: Atom/Dumbbel and Ru/Co ordering in derivatives of YCo5, Cryst. Growth Des. 17 (2017) 1610-1619.

47). N. Mounet, M. Gibertini, P. Schwaller, D. Campi, A. Merkys, A. Marrazzo, T. Sohier, I. E. Castelli, A. Cepellotti, G. Pizzi and N. Marzari, Two-dimensional materials from high-throughput computational exfoliation of experimentally known compounds, Nature Nanotechn. 13 (2018) 246-252.

48). K. B. Joshi, U. Paliwal, K. L. Galav, D. K. Trivedi and T. Bredow, Study of MgxCd1-xO applying density functional theory: Stability, structural phase transition and electronic properties, J. Solid State Chem. 204 (2013) 367-382.

49). R. S. Koster, C. M. Fang, M. Dijkstra, A. van Blaaderen and M. A. van Huis, Stablization of rock salt ZnO nanocrystals by low-energy surfaces and Mg additions: A first-principles study, J. Phys. Chem. C 119 (2015) 5648-5656.